Differential uncertainty analysis for evaluating the accuracy of S-parameter retrieval methods for electromagnetic properties of metamaterial slabs

Ugur Cem Hasar,[1,2,*] Joaquim J. Barroso,[3] Cumali Sabah,[4] Yunus Kaya,[1] and Mehmet Ertugrul[1,2]

[1]*Department of Electrical and Electronics Engineering, Ataturk University, 25240 Erzurum, Turkey*
[2]*Center for Research and Application of Nanoscience and Nanoengineering, Ataturk University, 25240 Erzurum, Turkey*
[3]*Associated Plasma Laboratory, National Institute for Space Research 12227-010 São José dos Campos, SP, Brazil*
[4]*Department of Electrical and Electronics Engineering, Middle East Technical University-Northern Cyprus Campus, Kalkanli, Guzelyurt, KKTC, Mersin 10, Turkey*
[*]*ugurcem@atauni.edu.tr*

Abstract: We apply a complete uncertainty analysis, not studied in the literature, to investigate the dependences of retrieved electromagnetic properties of two MM slabs (the first one with only split-ring resonators (SRRs) and the second with SRRs and a continuous wire) with single-band and dual-band resonating properties on the measured/simulated scattering parameters, the slab length, and the operating frequency. Such an analysis is necessary for the selection of a suitable retrieval method together with the correct examination of exotic properties of MM slabs especially in their resonance regions. For this analysis, a differential uncertainty model is developed to monitor minute changes in the dependent variables (electromagnetic properties of MM slabs) in functions of independent variables (scattering (S-) parameters, the slab length, and the operating frequency). Two complementary approaches (the analytical approach and the dispersion model approach) each with different strengths are utilized to retrieve the electromagnetic properties of various MM slabs, which are needed for the application of the uncertainty analysis. We note the following important results from our investigation. First, uncertainties in the retrieved electromagnetic properties of the analyzed MM slabs drastically increase when values of electromagnetic properties shrink to zero or near resonance regions where S-parameters exhibit rapid changes. Second, any low-loss or medium-loss inside the MM slabs due to an imperfect dielectric substrate or a finite conductivity of metals can decrease these uncertainties near resonance regions because these losses hinder abrupt changes in S-parameters. Finally, we note that precise information of especially the slab length and the operating frequency is a prerequisite for accurate analysis of exotic electromagnetic properties of MM slabs (especially multiband MM slabs) near resonance regions.

OCIS codes: (160.3918) Metamaterials; (290.3030) Index measurements.

References and links

1. V. G. Veselago, "The electrodynamics of substances with simultaneously negative values of ε and μ ," Sov. Phys. Uspekhi **10**, 509–514 (1968).
2. J. B. Pendry, "Negative refraction makes a perfect lens," Phys. Rev. Lett. **85**(18), 3966–3969 (2000).
3. R. A. Shelby, D. R. Smith, and S. Schultz, "Experimental verification of a negative index of refraction," Science **292**(5514), 77–79 (2001).

#174527 - $15.00 USD Received 17 Aug 2012; revised 15 Oct 2012; accepted 22 Oct 2012; published 13 Dec 2012

4. M. Choi, S. H. Lee, Y. Kim, S. B. Kang, J. Shin, M. H. Kwak, K. Y. Kang, Y. H. Lee, N. Park, and B. Min, "A terahertz metamaterial with unnaturally high refractive index," Nature **470**(7334), 369–373 (2011).
5. W. H. Wee and J. B. Pendry, "Universal evolution of perfect lenses," Phys. Rev. Lett. **106**(16), 165503 (2011).
6. D. R. Smith, W. J. Padilla, D. C. Vier, S. C. Nemat-Nasser, and S. Schultz, "Composite medium with simultaneously negative permeability and permittivity," Phys. Rev. Lett. **84**(18), 4184–4187 (2000).
7. J. B. Pendry, D. Schurig, and D. R. Smith, "Controlling electromagnetic fields," Science **312**(5781), 1780–1782 (2006).
8. R. Melik, E. Unal, N. K. Perkgoz, C. Puttlitz, and H. V. Demir, "Metamaterial-based wireless strain sensors," Appl. Phys. Lett. **95**(1), 011106 (2009).
9. L. Jelinek, R. Marques, and M. J. Freire, "Accurate modeling of split ring metamaterial lenses for magnetic resonance imaging applications," J. Appl. Phys. **105**(2), 024907 (2009).
10. C. Helgert, C. Rockstuhl, C. Etrich, C. Menzel, E.-B. Kley, A. Tunnermann, F. Lederer, and T. Pertsch, "effective properties of amorphous metamaterials," Phys. Rev. B **79**(23), 233107 (2009).
11. D. A. Pawlak, S. Turczynski, M. Gajc, K. Kolodziejak, R. Diduszko, K. Rozniatowski, J. Smalc, and I. Vendik, "How far are we from making metamaterials by self-organization? The microstructure of highly anisotropic particles with an SRR-like geometry," Adv. Funct. Mater. **20**(7), 1116–1124 (2010).
12. R. E. Collin, *Field Theory of Guided Waves* (Wiley-IEEE Press, 1990).
13. J. B. Pendry, A. J. Holden, D. J. Robbins, and W. J. Stewart, "Low frequency plasmons in thin-wire structures," J. Phys. Condens. Matter **10**(22), 4785–4809 (1998).
14. J. B. Pendry, A. J. Holden, D. J. Robbins, and W. J. Stewart, "Magnetism from conductors and enhanced nonlinear phenomena," IEEE Trans. Microw. Theory Tech. **47**(11), 2075–2084 (1999).
15. K. Aydin, Z. Li, M. Hudlicka, S. A. Tretyakov, and E. Ozbay, "Transmission characteristics of bianisotropic metamaterials based on omega shaped metallic inclusions," New J. Phys. **9**(9), 326 (2007).
16. C. Sabah, "Multiband planar metamaterials," Microw. Opt. Technol. Lett. **53**(10), 2255–2258 (2011).
17. Q. Zhao, L. Kang, B. Du, B. Li, J. Zhou, H. Tang, X. Liang, and B. Zhang, "Electrically tunable negative permeability metamaterials based on nematic liquid crystals," Appl. Phys. Lett. **90**(1), 011112 (2007).
18. H. Nemec, P. Kuzel, F. Kadlec, C. Kadlec, R. Yahiaoui, and P. Mounaix, "Tunable terahertz metamaterials with negative permeability," Phys. Rev. B **79**, 241108(R) (2009).
19. C. Menzel, C. Rockstuhl, T. Paul, F. Lederer, and T. Pertsch, "Retrieving effective parameters for metamaterials at oblique incidence," Phys. Rev. B **77**(19), 195328 (2008).
20. A. Taflove and S. C. Hagness, *Computational Electrodynamics: The Finite-Difference Time-Domain Method* (Artech House, 2000).
21. D. R. Smith, S. Schultz, P. Markos, and C. M. Soukoulis, "Determination of effective permittivity and permeability of metamaterials from reflection and transmission coefficients," Phys. Rev. B **65**(19), 195104 (2002).
22. M. Notomi, "Theory of light propagation in strongly modulated photonic crystals: Refractionlike behavior in the vicinity of the photonic band gap," Phys. Rev. B **62**(16), 10696–10705 (2000).
23. T. Paul, C. Menzel, W. Smigaj, C. Rockstuhl, P. Lalanne, and F. Lederer, "Reflection and transmission of light at periodic layered metamaterial films," Phys. Rev. B **84**(11), 115142 (2011).
24. Z. Li, K. Aydin, and E. Ozbay, "Determination of the effective constitutive parameters of bianisotropic metamaterials from reflection and transmission coefficients," Phys. Rev. E Stat. Nonlin. Soft Matter Phys. **79**(2), 026610 (2009).
25. D. R. Smith, D. C. Vier, T. Koschny, and C. M. Soukoulis, "Electromagnetic parameter retrieval from inhomogeneous metamaterials," Phys. Rev. E Stat. Nonlin. Soft Matter Phys. **71**(3 3 Pt 2B), 036617 (2005).
26. P. Markos and C. M. Soukoulis, "Transmission properties and effective electromagnetic parameters of double negative metamaterials," Opt. Express **11**(7), 649–661 (2003).
27. M. Bozzi, L. Perregrini, J. Weinzierl, and C. Winnewisser, "Efficient analysis of quasi-optical filters by a hybrid MoM/Bi-RME method," IEEE Trans. Antenn. Propag. **49**(7), 1054–1064 (2001).
28. Z. H. Jiang, J. A. Bossard, X. Wang, and D. H. Werner, "Synthesizing metamaterials with angularly independent effective medium properties based on an anisotropic parameter retrieval technique coupled with a genetic algorithm," J. Appl. Phys. **109**(1), 013515 (2011).
29. T. Driscoll, D. N. Basov, W. J. Padilla, J. J. Mock, and D. R. Smith, "Electromagnetic characterization of planar metamaterials by oblique angle spectroscopic measurements," Phys. Rev. B **75**(11), 115114 (2007).
30. D. R. Smith, D. Schurig, and J. J. Mock, "Characterization of a planar artificial magnetic metamaterial surface," Phys. Rev. E Stat. Nonlin. Soft Matter Phys. **74**(3), 036604 (2006).
31. K. B. Alici and E. Ozbay, "Oblique response of a split-ring-resonator-based left-handed metamaterial slab," Opt. Lett. **34**(15), 2294–2296 (2009).
32. X. Chen, B.-I. Wu, J. A. Kong, and T. M. Grzegorczyk, "Retrieval of the effective constitutive parameters of bianisotropic metamaterials," Phys. Rev. E Stat. Nonlin. Soft Matter Phys. **71**(4), 046610 (2005).
33. U. C. Hasar and J. J. Barroso, "Retrieval approach for determination of forward and backward wave impedances of bianisotropic metamaterials," Prog. Electromagn. Res. **112**, 109–124 (2011).
34. R. Marqués, F. Medina, and R. Rafii-El-Idrissi, "Role of bianisotropy in negative permeability and left-handed metamaterials," Phys. Rev. B **65**(14), 144440 (2002).
35. A. Alù, "First-principles homogenization theory for periodic metamaterials," Phys. Rev. B **84**(7), 075153 (2011).
36. A. M. Nicolson and G. Ross, "Measurement of the intrinsic properties of materials by time–domain techniques," IEEE Trans. Instrum. Meas. **19**(4), 377–382 (1970).

#174527 - $15.00 USD Received 17 Aug 2012; revised 15 Oct 2012; accepted 22 Oct 2012; published 13 Dec 2012

37. X. Chen, T. M. Grzegorczyk, B.-I. Wu, J. Pacheco, Jr., and J. A. Kong, "Robust method to retrieve the constitutive effective parameters of metamaterials," Phys. Rev. E Stat. Nonlin. Soft Matter Phys. **70**(1), 016608 (2004).
38. U. C. Hasar, "A microwave method for accurate and stable retrieval of constitutive parameters of low- and medium-loss materials," IEEE Microw. Wirel. Compon. Lett. **20**(12), 696–698 (2010).
39. U. C. Hasar, "Procedure for accurate and stable constitutive parameters extraction of materials at microwave frequencies," Prog. Electromagn. Res. **109**, 107–121 (2010).
40. J. Qi, H. Kettunen, H. Wallen, and A. Sihvola, "Compensation of Fabry-Perot resonances in homogenization of dielectric composites," IEEE Antennas Wireless Propag. Lett. **9**, 1057–1060 (2010).
41. X.-X. Liu, D. A. Powell, and A. Alu, "Correcting the Fabry-Perot artifacts in metamaterial retrieval procedures," Phys. Rev. B **84**(23), 235106 (2011).
42. W. B. Weir, "Automatic measurement of complex dielectric constant and permeability at microwave frequencies," Proc. IEEE **62**(1), 33–36 (1974).
43. A. H. Muqaibel and A. Safaai-Jazi, "A new formulation for characterization of materials based on measured insertion transfer function," IEEE Trans. Microw. Theory Tech. **51**(8), 1946–1951 (2003).
44. S. Xia, Z. Xu, and X. Wei, "Thickness-induced resonance-based complex permittivity measurement technique for barium strontium titanate ceramics at microwave frequency," Rev. Sci. Instrum. **80**(11), 114703 (2009).
45. O. Büyüköztürk, T.-Y. Yu, and J. A. Ortega, "A methodology for determining complex permittivity of construction materials based on transmission-only coherent, wide-bandwidth free-space measurements," Cement Concr. Compos. **28**(4), 349–359 (2006).
46. U. C. Hasar, "Unique permittivity determination of low-loss dielectric materials from transmission measurements at microwave frequencies," Prog. Electromagn. Res. **107**, 31–46 (2010).
47. Z. Szabo, G.-H. Park, R. Hedge, and E.-P. Li, "Unique extraction of metamaterial parameters based on Kramers-Kronig relationship," IEEE Trans. Microw. Theory Tech. **58**(10), 2646–2653 (2010).
48. V. V. Varadan and R. Ro, "Unique retrieval of complex permittivity and permeability of dispersive materials from reflection and transmitted fields by enforcing causality," IEEE Trans. Microw. Theory Tech. **55**(10), 2224–2230 (2007).
49. J. J. Barroso and U. C. Hasar, "Resolving phase ambiguity in the inverse problem of transmission/reflection measurement methods," Int. J. Infrared Millim. Waves **32**(6), 857–866 (2011).
50. U. C. Hasar, J. J. Barroso, C. Sabah, and Y. Kaya, "Resolving phase ambiguity in the inverse problem of reflection-only measurement methods," Prog. Electromagn. Res. **129**, 405–420 (2012).
51. O. Luukkonen, S. I. Maslovski, and S. A. Tretyakov, "A tespwise Nicolson-Ross-Weir-based material parameter extraction method," IEEE Antennas Wirel. Propag. Lett. **10**, 1295–1298 (2011).
52. B. Kapilevih and B. Litvak, "THz characterization of high-dielectric constant materials using double-layer sample," Microw. Opt. Technol. Lett. **49**(6), 1388–1391 (2007).
53. U. C. Hasar and I. Y. Ozbek, "Complex permittivity determination of lossy materials at millimeter and terahertz frequencies using free-space amplitude measurements," J. Electromagn. Waves Appl. **25**(14-15), 2100–2109 (2011).
54. U. C. Hasar and A. Abusoglu, "Using millimeter and terahertz frequencies for complex permittivity retrieval of low-loss materials," J. Electromagn. Waves Appl. **25**(17-18), 2389–2398 (2011).
55. B. Kapilevich, Y. Pinhasi, and B. Litvak, "Measurement of complex permittivity of lossy materials in free space using matched THz power meter," Int. J. Infrared Millim. Waves **32**(12), 1446–1456 (2011).
56. J. Zhou, Th. Koschny, M. Kafesaki, E. N. Economou, J. B. Pendry, and C. M. Soukoulis, "Saturation of the magnetic response of split-ring resonators at optical frequencies," Phys. Rev. Lett. **95**(22), 223902 (2005).
57. E. Pshenay-Severin, F. Setzpfandt, C. Helgert, U. Hubner, C. Menzel, A. Chipouline, C. Rockstuhl, A. Tunnermann, F. Lederer, and T. Pertsch, "Experimental determination of the dispersion relation of light in metamaterials by white-light interferometry," J. Opt. Soc. Am. B **27**(4), 660–666 (2010).
58. C. Sabah, "Multiband metamaterials based on multiple concentric open ring resonators topology," IEEE J. Sel. Topics Quantum Electron. 2012 (DOI#: 10.1109/JSTQE.2012.2193875).
59. C. Sabah, "Multi-resonant metamaterial design based on concentric V -shaped magnetic resonators," J. Electromagn. Waves Appl. **26**(8-9), 1105–1115 (2012).
60. D. M. Pozar, *Microwave Engineering* (Wiley, Hoboken, NJ, 2005).
61. T. Weiland, R. Schuhmann, R. B. Greegor, C. G. Parazzoli, A. M. Vetter, D. R. Smith, D. C. Vier, and S. Schultz, "Ab *initio* numerical simulation of left-handed metamaterials: Comparison of calculations and experiments," J. Appl. Phys. **90**(10), 5419–5424 (2001).
62. G. Lubkowski, B. Bandlow, R. Schuhmann, and T. Weiland, "Effective modeling of double negative metamaterial macrostructures," IEEE Trans. Microw. Theory Tech. **57**(5), 1136–1146 (2009).
63. R. W. Ziolkowski and E. Heyman, "Wave propagation in media having negative permittivity and permeability," Phys. Rev. E Stat. Nonlin. Soft Matter Phys. **64**(5), 056625 (2001).
64. T. J. Cui and J. A. Kong, "Time-domain electromagnetic energy in a frequency-dispersive left-handed medium," Phys. Rev. B **70**(20), 205106 (2004).
65. C. Sabah and S. Uckun, "Multilayer system of Lorentz/Drude type metamaterials with dielectric slabs and its application to electromagnetic filters," Prog. Electromagn. Res. **91**, 349–364 (2009).
66. J. Baker-Jarvis, R. G. Geyer, and P. D. Domich, "A nonlinear least-squares solution with causality constrains applied to transmission line permittivity and permeability determination," IEEE Trans. Instrum. Meas. **41**(5), 646–652 (1992).
67. S. Xu, L. Yang, L. Huang, and H. Chen, "Experimental measurement method to determine the permittivity of extra thin materials using resonating metamaterials," Prog. Electromagn. Res. **120**, 327–337 (2011).

#174527 - $15.00 USD Received 17 Aug 2012; revised 15 Oct 2012; accepted 22 Oct 2012; published 13 Dec 2012

68. C. Alexander and M. Sadiku, *Fundamentals of Electric Circuits* (McGraw-Hill, 2002).
69. U. C. Hasar, I. Y. Ozbek, E. A. Oral, T. Karacali, and H. Efeoglu, "The effect of silicon loss and fabrication tolerance on spectral properties of porous silicon Fabry-Perot cavities in sensing applications," Opt. Express **20**(20), 22208–22223 (2012).
70. G. Lubkowski, R. Schuhmann, and T. Weiland, "Extraction of effective metamaterial parameters by parameter fitting of dispersive models," Microw. Opt. Technol. Lett. **49**(2), 285–288 (2007).
71. R. Storn and K. Price, "Differential evaluation–A simple and efficient heuristic for global optimization over continuous spaces," J. Glob. Optim. **11**(4), 341–359 (1997).
72. K. Price, R. Storn, and J. Lampinen, *Differential Evolution - A Practical Approach to Global Optimization* (Springer, 2005).
73. K. Price and R. Storn, "Differential evaluation (DE) for continuous function optimization," http://www.icsi.berkeley.edu/~storn/code.html.
74. The MathWorks, http://www.mathworks.com.
75. J. Baker–Jarvis, E. J. Vanzura, and W. A. Kissick, "Improved technique for determining complex permittivity with the transmission/reflection method," IEEE Trans. Microw. Theory Tech. **38**(8), 1096–1103 (1990).
76. A. H. Boughriet, C. Legrand, and A. Chapoton, "Noniterative stable transmission/reflection method for low-loss material complex permittivity determination," IEEE Trans. Microw. Theory Tech. **45**(1), 52–57 (1997).
77. U. C. Hasar and C. R. Westgate, "A broadband and stable method for unique complex permittivity determination of low-loss materials," IEEE Trans. Microw. Theory Tech. **57**(2), 471–477 (2009).
78. J. J. Barroso and A. L. de Paula, "Retrieval of permittivity and permeability of homogeneous materials from scattering parameters," J. Electromagn. Waves Appl. **24**(11-12), 1563–1574 (2010).
79. K. Chalapat, K. Sarvala, J. Li, and G. S. Paraoanu, "Wideband reference-plane invariant method for measuring electromagnetic parameters of materials," IEEE Trans. Microw. Theory Tech. **57**(9), 2257–2267 (2009).
80. S. J. Kline and F. A. McClintock, "Describing uncertainties in single–sample experiments," Mech. Eng. **75**, 3 (1953).
81. J. Baker–Jarvis, M. D. Janezic, J. H. Grosvenor, Jr., and R. G. Geyer, "Transmission/reflection and short–circuit line methods for measuring permittivity and permeability," NIST, Boulder, CO, Tech. Note 1355, (1992).
82. G. B. Arfken, H. J. Weber, and F. E. Harris, *Mathematical Methods for Physicists: A Comprehensive Guide* (Academic Press, 2005).
83. E. Kreyszig, *Advanced Engineering Mathematics* (Wiley, 2006).
84. H. J. Pain, *The Physics of Vibrations and Waves* (Wiley, 2008).

1. Introduction

Metamaterials (MMs) have attracted a huge research interest to scientific community in recent years since they have unusual electromagnetic properties not available in conventional materials [1–3], such as negative refraction [4], perfect lenses [2,5], potential applications in invisibility cloaks [6,7], sensors [8], and resonators [9]. MMs are artificial media composed of periodically [2–7] or amorphously [10,11] oriented inhomogeneities (meta-atoms) embedded in a host conventional material. Periodically oriented MMs are similar to artificial dielectrics obtained by arranging a large number of identical conducting obstacles, simulating the behavior of a molecule (or a group of molecules) in an ordinary dielectric, in a regular three-dimensional (3-D) pattern [12]. MMs are composed of unit cells with either metallic structures with various geometries on a host dielectric medium (metallic cut wires, split-ring-resonators (SRRs), etc [13–16].) or non-metallic ones [17,18]. Based on the optical property of the MM unit cells, simultaneous negative effective permittivity and negative effective permeability (or any of them) at a certain frequency band can be achievable. For instance, while metallic wire cut periodic array (continuous wires) behaves like plasma and possesses a negative effective permittivity over a broadband [13], SRR periodic array produces a negative effective permeability within a limited frequency range [14].

A brute force approach for analyzing the interaction of electromagnetic fields with MMs is to rigorously solve the macroscopic Maxwell's equations considering inhomogeneous permittivity and permeability [19] by using standard numerical techniques such as the finite-difference time-domain method [20]. In this circumstance, at a given frequency, any material (continuous or non-continuous) supporting only one propagating mode will generally exhibit a well-defined refractive index (n) [21,22], but not a normalized wave impedance (z) which highly depends upon the overall size of the MM [21]. In some circumstances, however, the complex response of MMs to electromagnetic waves can be analyzed, as an equal problem, by the effective (continuous) medium approach considering a MM slab as a continuous material if the operating wavelength inside the MM slab is much larger than the spacing between the composite components (scatterers) and the size of respective components of the

#174527 - $15.00 USD Received 17 Aug 2012; revised 15 Oct 2012; accepted 22 Oct 2012; published 13 Dec 2012

MM slab [23–26]. In latter circumstances in which effective medium approach could be applied, not only n but also z will have well-defined values not depending on the overall size of the MM [23].

Care must be given in using the continuous medium approximation. First, the electromagnetic field near the MM slab must satisfy the Floquet's theorem and thus can be expanded in a set of transverse-magnetic and transverse-electric modes (Floquet or Bloch modes) [27]. If the periodicity is small enough, higher-order Floquet modes are evanescent in the propagation direction, and reflected and transmitted fields at a certain distance from the structure are essentially a combination of zeroth order (fundamental) modes. Therefore, plane waves incident to a MM slab can be analyzed as if it is a homogeneous slab. Second, retrieved constitutive parameters of the analyzed MM slabs depend on the definite direction of the wave incident to the MM slab, and thus may be termed as wave parameters [19,24,28–33]. This dependence of optical parameters on the wave vector arises due to anisotropy or spatial dispersion [19].

In order to probe the electromagnetic properties of metamaterials, there are currently four methods. The first method (qualitative effective medium theory) determines the electromagnetic properties of MM slabs by using approximate analytical models [34]. Although yielding accurate results for simple MM structures, this method is not much practicable for complex MM structures since it requires the preparation of four different MM slabs [31], and thus its accuracy may decrease with any inaccuracy in the fabricated MM slabs. The second method, which is suitable for numerical simulations but not in experiments, is to numerically calculate the ratios of the electric and magnetic fields over surfaces and edges inside MMs [13]. The third method is to propose new homogenization methods by collecting the advantages of currently available homogenization schemes [35]. The final and most prevalently used method is to retrieve the electromagnetic properties of MM slabs from measured/simulated scattering (S-) parameters [21,24,25,29,32,33,36,37]. It is suitable for both numerical simulations and experimental measurements. In applying this methodology, first S-parameters, containing amplitude and phase information, of the analyzed MM slab are obtained. Then, these parameters are substituted into theoretically derived expressions to determine the electromagnetic properties of that MM slab. Although new and high-capable state of the art network analyzers are produced, and these analyzers perform a wide band frequency measurements in a few seconds, methods using measured/simulated S-parameters suffer from a few drawbacks for accurate retrieval of electromagnetic properties of MM slabs. The first disadvantage is the presence of Fabry-Perot resonances, which is expected to be a constraint within a narrow frequency band. There are some methods available in the literature to overcome this drawback [38–41]. Another problem is the non-unique retrieval of electromagnetic properties of MM slabs as a result of the presence of complex exponentials in S-parameters. The methods in [42–51] can be employed for different purposes to remove this disadvantage. The final drawback of electromagnetic retrieval of MM slabs by methods based on S-parameters is the unfeasible measurement of the phase of S-parameters at very high frequencies [29,52–57]. As a solution to this problem, amplitude-only Fresnel measurements at multiple frequencies could be utilized [29,52–56]. Because, in the region of negative refraction, real parts of both relative complex permittivity (ε_r) and relative complex permeability (μ_r) depend mainly on the phase measurements, as another solution, complex S-parameter measurements based on an interferometric approach are more appealing for sensitive measurements [57].

After performing a survey over literature, we have noted that most of the S-parameter extraction methods [21,24–26,29,32,37,57] for determination of electromagnetic properties of MM slabs do not consider a full and descriptive analysis about the effect of any uncertainty in measured S-parameters, and the thickness of the analyzed MM slabs on the retrieved properties. The sensitivity analysis of the retrieval method [37] does not go beyond interrogating the effect of measured transmission S-parameter on the retrieved wave impedance of MM slabs. Besides, the uncertainty analysis in [57] is limited in the sense that it

#174527 - $15.00 USD Received 17 Aug 2012; revised 15 Oct 2012; accepted 22 Oct 2012; published 13 Dec 2012

only analyzes the effect of measured S-parameters on the extracted n (not the effect of MM slab thickness and operating frequency). A complete uncertainty analysis is very useful in selecting the most appropriate S-parameter method for accurate retrieval of electromagnetic properties of MM slabs with a given configuration. In addition to the uncertainties of S-parameters and the thickness, investigating the effect of any uncertainty in the operating wavelength seems to be useful for multiband MM structures [16,58,59]. In this research paper, we present the results of a complete uncertainty analysis for examining the dependence of retrieved electromagnetic properties of MM slabs on the uncertainties in S-parameters, the thickness and also the operating wavelength.

2. Scattering parameters of MM slabs

A typical problem of determining effective electromagnetic properties of MM slabs with different properties using forward and backward S-parameter measurements/simulations is depicted in Figs. 1 and 2. A plane wave polarized in the z direction propagates along the x direction and is incident upon each cubic MM cell in Figs. 1 and 2. While the MM cells in Fig. 1 are single-band (SB), those in Fig. 2 are dual-band (DB) [16,58,59]. The MM cell (SB SRR MM slab) in Fig. 1(a) is composed of only edge-coupled SRRs asymmetric with respect to x axis (symmetric to the vertical axis z) whereas the MM cell (DB SRR MM slab) in Fig. 2(a) consists two concentric open ring resonators symmetric with respect to x axis. Besides, the MM structure (SB Composite MM slab) in Fig. 1(b) has asymmetric edge-coupled SRRs as well as a continuous wire in the direction of E-field, and the MM structure (DB Composite MM slab) in Fig. 2(b) has two concentric open ring resonators together with a continuous wire in the direction of E-field. Of these structures, those in Figs. 1(b) and 2(b) show negative refractive index within a certain frequency range or certain frequency ranges [21].

By assuming that each cell in Figs. 1 and 2 is reciprocal (because it is composed of passive components [60]) and that the reference harmonic time dependence is $\exp(-i\omega t)$, implying that imaginary parts of ε_r and μ_r are both greater than zero for a passive medium in the investigated frequency region, forward and backward reflection and transmission S-parameters for each homogeneous MM slab (actually, MMs have an inhomogeneous structure) in Figs. 1 and 2 can be written [21,26,36,37,42] after the application of boundary conditions of continuous transverse electric and magnetic field components at $x = 0$ and $x = d$

$$S_{11} = |S_{11}|e^{i\theta_{11}} = \frac{\Gamma\left(1-T^2\right)}{1-\Gamma^2T^2} = S_{22}, \quad S_{21} = |S_{21}|e^{i\theta_{21}} = \frac{T\left(1-\Gamma^2\right)}{1-\Gamma^2T^2} = S_{12}, \tag{1}$$

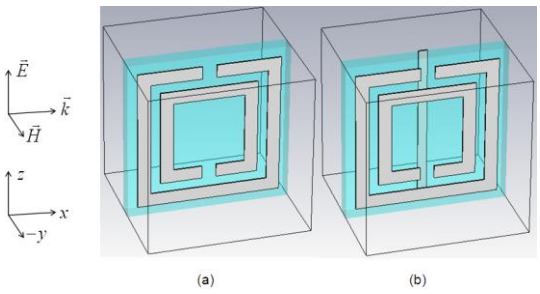

Fig. 1. Schematic view of a single cell of a metamaterial (a) with SRRs only and (b) with SRRs and a wire.

#174527 - $15.00 USD Received 17 Aug 2012; revised 15 Oct 2012; accepted 22 Oct 2012; published 13 Dec 2012

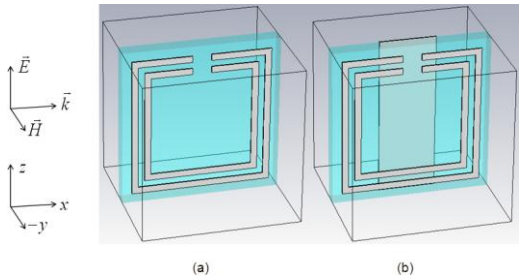

Fig. 2. Schematic view of a single cell of a metamaterial (a) with concentric open ring resonators only and (b) with concentric open ring resonators and a wire.

where Γ and T are, respectively, the (intrinsic) reflection coefficient at the air-MM slab interface and the propagation factor through the MM slab. Their expressions read as

$$\Gamma = (z-1)/(z+1), \quad T = \exp(ik_0 nd), \quad k_0 = 2\pi f/c. \tag{2}$$

Here, z and n are, respectively, the normalized wave impedance and the refractive index of the MM slab, k_0 the free-space wavenumber, d the thickness of the MM slab, f the operating frequency, and c the velocity of light in vacuum.

3. Simulation results

We use the unit cell dimensions in [25] as for the dimensions of SB unit MM cells in Fig. 1 to simulate S-parameters whereas we analyze a different structure for the DB unit MM cells in Fig. 2. Each unit cell in Figs. 1 and 2 is cubic with a cell dimension of $d = 2.5$ mm. A 0.25 mm thick substrate has the following properties $\varepsilon_{rs} = 4.4$ and loss tangent of 0.0002 for the cells in Fig. 1, and $\varepsilon_{rs} = 10.2$ and loss tangent of 0.0023 for the cells in Fig. 2. Perfect electric conductor (PEC) SRRs and wire, each having a thickness of 17 μm, are assumed to be positioned on opposite sides of the substrate of each cell in Figs. 1 and 2. The wire height is 2.5 mm for each cell in Figs. 1 and 2, and the wire width of the cells in Fig. 1 is 0.14 mm and is 0.90 mm for the cells in Fig. 2. The outer ring length of the SRR in each cell in Figs. 1 and 2 is 2.2 mm, and while both rings in Fig. 1 have a linewidth of 0.2 mm, those in Fig. 2 have a linewidth of 0.1 mm. The gap open in the x direction in each ring in Figs. 1 and 2 is 0.3 mm, and the gap between the inner and outer rings is 0.15 mm for cells in Fig. 1 and 0.10 mm for the cells in Fig. 2. These unit cells are denoted as low-loss MM unit cells in the explanation of the results in our manuscript. When the loss tangent of substrate of MM slabs is increased to 0.02, and PEC of SRRs and wire is changed to copper with an electrical conductivity of 5.8×10^7 (S/m), they are designated as lossy unit cells for referencing the results.

We utilize the CST Microwave Studio simulation program based on finite integration technique [61] to simulate S-parameters for each unit cell in Figs. 1 and 2. The structure is excited by an electromagnetic plane wave with an electric field vector $\vec{E}$ oriented along z-axis, magnetic field vector $\vec{H}$ oriented along $-y$-axis, and propagation vector $\vec{k}$ oriented along x-axis. Whereas waveguide ports are assumed perpendicular to the x-direction, periodic boundary conditions are used along y- and z-directions [62]. For brevity, simulated S-parameters of only lossy cells in Figs. 1 and 2 are shown in Figs. 3 and 4.

#174527 - $15.00 USD Received 17 Aug 2012; revised 15 Oct 2012; accepted 22 Oct 2012; published 13 Dec 2012

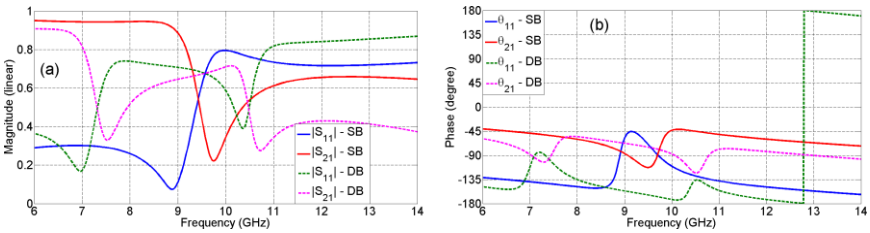

Fig. 3. (a) Magnitude and (b) phase of the simulated S-parameters for the lossy SB&DB SRR MM slabs.

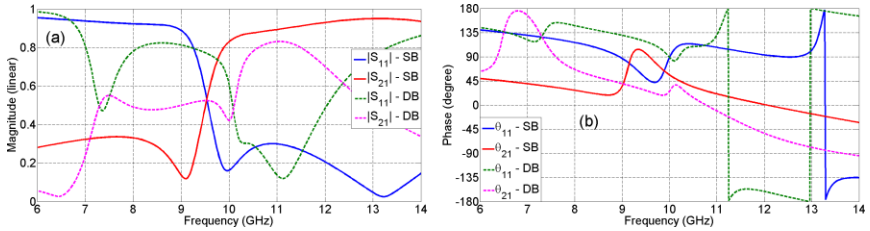

Fig. 4. (a) Magnitude and (b) phase of the simulated S-parameters for the lossy SB&DB Composite MM slabs.

4. Retrieved electromagnetic properties

In this section, we present the retrieved electromagnetic properties of homogenized MM slabs with details of their geometries discussed in Section 3 using their simulated S-parameters (only lossy ones are shown in Figs. 3 and 4). We apply two different approaches in the retrieval process. The first approach is based upon extraction of electromagnetic properties from explicit analytical expressions [37], while the second approach uses dispersion models (Lorentz and Drude types [3,14,63–66]) to predict accurate electromagnetic properties [66]. The advantages and drawbacks of each approach will be discussed where appropriate.

4.1. The analytical approach

The analytical approach [37] extracts the electromagnetic properties of homogenized MMs in Figs. 1 and 2 using explicit expressions. To apply this approach, from Eqs. (1) and (2), z and n are determined by simulated/measured S-parameters as

$$z = \mp\sqrt{\frac{(1+S_{11})^2 - S_{21}^2}{(1-S_{11})^2 - S_{21}^2}}, \quad T = \frac{S_{21}}{1-S_{11}(z-1)/(z+1)}, \tag{3}$$

$$n = \left[\mp(\ln T)'' \mp 2\pi m - i(\ln T)'\right] / (k_0 d), \quad m = 0,1,2,3... \tag{4}$$

where m denotes the branch index value and, from now on, primes and double primes denote real and imaginary parts of a complex quantity, respectively.

It is known that for a homogenized MM slab, its z and n'' can be uniquely retrieved from S-parameter measurements [21,26,37] without considering the m value. For a passive (source-free) medium, the sign before the square root in the expression of z in Eq. (3) can be ascertained by $z' > 0$ [21]. Besides, the correct choice of m for unique retrieval of n' can be realized by different techniques [42–51]. Finally, ε_r and μ_r are computed from

$$\varepsilon_r = n/z, \quad \mu_r = nz. \tag{5}$$

Utilizing the expressions in Eqs. (3)-(5) and simulated S-parameters, for each low-loss and lossy MM slab in Figs. 1 and 2, we first retrieve z and n and then determine ε_r and

#174527 - $15.00 USD Received 17 Aug 2012; revised 15 Oct 2012; accepted 22 Oct 2012; published 13 Dec 2012

μ_r . For the purpose of conciseness, we show these parameters of only the lossy SB&DB MM slabs in Figs. 5, 6, 7, and 8 using their simulated S-parameters in Figs. 3 and 4. The results and discussion of the uncertainty analysis for low-loss MM slabs are presented in next section. Note that because our formulation in Section 2 assumes a time dependence of $\exp(-i\omega t)$ while the CST software package considers the $\exp(+i\omega t)$ for its computations, we negated the phase value of simulated S-parameters for the retrieval of electromagnetic properties in the remainder part of our study.

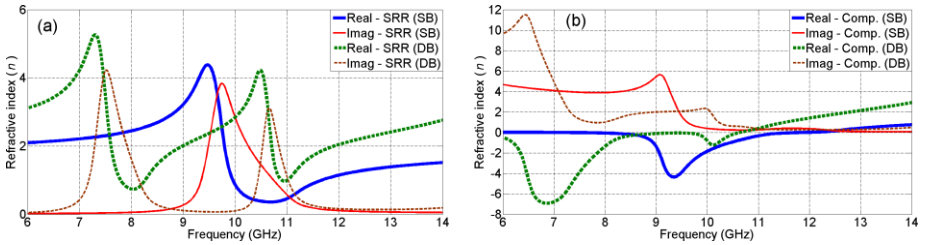

Fig. 5. Real and imaginary parts of retrieved refractive index of the lossy SB&DB (a) SRR MM slab and (b) Composite MM slab using the analytical approach.

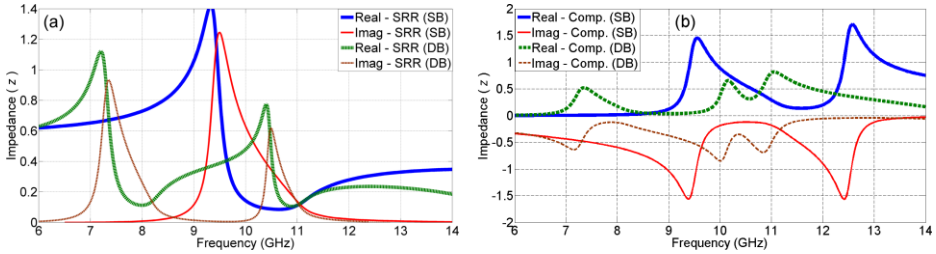

Fig. 6. Real and imaginary parts of retrieved wave impedance of the lossy SB&DB (a) SRR MM slab and (b) Composite MM slab using the analytical approach.

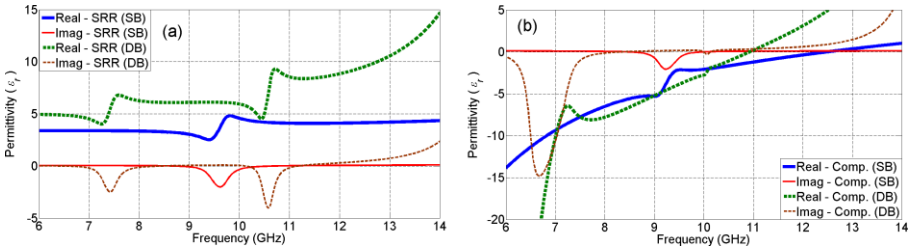

Fig. 7. Real and imaginary parts of retrieved permittivity of the lossy SB&DB (a) SRR MM slab and (b) Composite MM slab using the analytical approach.

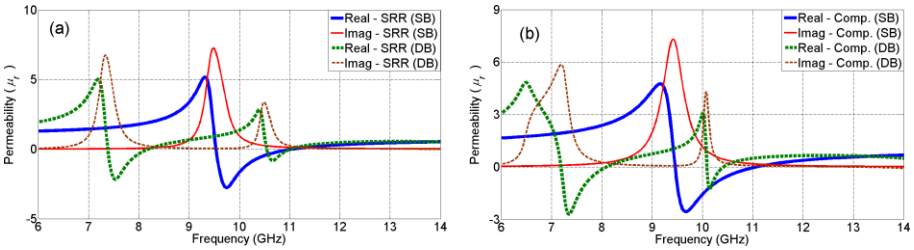

Fig. 8. Real and imaginary parts of retrieved permeability of the lossy SB&DB (a) SRR MM slab and (b) Composite MM slab using the analytical approach.

#174527 - $15.00 USD Received 17 Aug 2012; revised 15 Oct 2012; accepted 22 Oct 2012; published 13 Dec 2012

The results and discussion of the uncertainty analysis for low-loss MM slabs are presented in next section. Note that because our formulation in Section 2 assumes a time dependence of $\exp(-i\omega t)$ while the CST software package considers the $\exp(+i\omega t)$ for its computations, we negated the phase value of simulated S-parameters for the retrieval of electromagnetic properties in the remainder part of our study.

It is noticed from Fig. 5 that the lossy SB&DB SRR MM slabs have only positive n' over the whole frequency band while the lossy SB&DB Composite MM slabs have a negative n' over some narrow frequency regions (approximately between 8 and 12 GHz for SB, 6.0-8.5 GHz and 9.5-10.5 GHz for DB). It is well-known that a MM structure composed of only SRRs cannot possess a negative n' [21,24]. In addition, it is seen from Figs. 5–8 that the dependences of retrieved n , z , ε_r , and μ_r of the lossy SB Composite MM slab are in good agreement with those of Fig. 3 in [25]. However, we note from Fig. 7 that the retrieved ε_r'' of all MM slabs violates the passivity condition ($\varepsilon_r'' > 0$) over a few frequency regions such as 7.0-8.0 GHz and 10.0-11.0 GHz for DB SRR MM slab. This problem (violation of locality conditions) is attributed to spatial dispersion effects arising from the discreteness of the conducting elements that are repeated periodically in a non-homogeneous metamaterial bulk, which thus behaves as a non-local medium, and is seen in other articles [24–26,62]. These effects mostly manifest for large ε_r and μ_r values, when the amplitude and phase of the fields inside MM slabs vary quickly. This leads to a strong non-uniformity in the current distribution and local fields in the unit cell, thus making it difficult for the numerical code to account for such strong field variations properly. Finally, we note from Figs. 7(a) and 7(b) that the inverted red Gaussian-like curve for ε_r'' of the SB SRR MM slab at $f \cong 9.7$ GHz is on the right side of a similar curve for ε_r'' of the SB Composite MM slab at $f \cong 9.25$ GHz. This circumstance arises from the fact that MM slabs can be considered as resonating structures [67–69], and thus their resonance frequencies downshift with the inclusion of any lossy sample such as cut wires.

The preceding discussions for the lossy SB&DB MM slabs are also valid for low-loss SB&DB MM slabs. Therefore, the dependences of n , z , ε_r , and μ_r for low-loss MM slabs are not shown for conciseness. Although the analytical approach extracts electromagnetic properties of MMs faster, it does not clean out and thus not tolerate the inaccuracies ($\varepsilon_r'' < 0$) arising when the accuracy of our simulation program is not so high.

4.2. The dispersion model approach

This approach overcomes the problem of the analytical approach, discussed above, by fitting the simulated S-parameters to those obtained from the Drude and Lorentz type dispersion models, which describe local continuous media. In this way, any limited accuracy of simulation programs is handled by optimizing this fitting. Based on the Drude and Lorentz type dispersion models, expressions of ε_r and μ_r for any MM cell in Fig. 1 read as

$$\varepsilon_r(\omega) = \varepsilon_\infty - \frac{\omega_{ep}^2}{\omega(\omega + i\,\delta_e)}, \qquad \mu_r(\omega) = \mu_\infty - \frac{(\mu_s - \mu_\infty)\omega_{mp}^2}{\omega(\omega + i\,\delta_m) - \omega_{mp}^2}, \tag{6}$$

where ε_∞ is the electric permittivity at the high frequency (theoretically at infinity), ω_{ep} the electronic plasma frequency, δ_e the electronic damping (due to collision) coefficient, μ_∞ (μ_s) the magnetic permeability at the high (low) frequency (theoretically at infinity (zero)), ω_{mp} the magnetic plasma (resonant) frequency, and δ_m the magnetic damping (due to collision) coefficient.

#174527 - $15.00 USD Received 17 Aug 2012; revised 15 Oct 2012; accepted 22 Oct 2012; published 13 Dec 2012

We note from Figs. 5–8 that there are two frequency regions at which the MM cells in Fig. 2 resonates (DB). Therefore, the expressions of ε_r and μ_r in Eq. (6) cannot reflect such multiple resonance phenomenon. To meet this demand, similar to the Eqs. (20) and (21) in [66], we changed the form of the expressions in Eq. (6) to

$$\varepsilon_r(\omega) = \varepsilon_\infty - \sum_{t=1}^{N} \frac{\omega_{ep(t)}^2}{\omega\left(\omega + i\,\delta_{e(t)}\right)}, \qquad \mu_r(\omega) = \sum_{t=1}^{N} \left[\mu_{\infty(t)} - \frac{\left(\mu_{s(t)} - \mu_{\infty(t)}\right)\omega_{mp(t)}^2}{\omega\left(\omega + i\,\delta_{m(t)}\right) - \omega_{mp(t)}^2} \right], \quad (7)$$

which is applicable to multi-band resonating MM slabs. Here, t is the index parameter and N denotes the total number of resonating band regions (e.g., for DB slabs, $N = 2$). For homogenized SB&DB SRR slabs, we set all ω_{ep} values to zero in Eqs. (6) and (7).

By accounting for the frequency dependences of the MM slabs in Figs. 1 and 2 (SB or DB), by substituting ε_r and μ_r in Eqs. (6) and (7), sequentially, into Eqs. (5), (2), and (1), and by minimizing the difference between the S-parameters obtained from simulation and from the homogenized-cell representation, it becomes possible to get error-removed electromagnetic properties as well as the values of the unknowns in Eqs. (6) and (7) [70]. In [70], the authors utilized the differential evolution (DE) algorithm which is based on vector differences (lower χ^2 value) for perturbing an older vector population to obtain a newer vector population [71,72]. Although it is faster and needs less number of iterations than Nonlinear-least squares based on Levenberg-Marquardt method and genetic algorithms, can be applicable to nonlinear, non-differentiable, and multidimensional continuous space functions, and does not make any assumption (if not, few assumptions) about the problem being optimized (metaheuristic algorithm), the DE algorithm requires correct selection of the differential weight (F), the crossover probability (CR), and the population size (NP). With different initial combinations of F, CR, and NP, the DE algorithm produces different results [73] for the same optimization problem. Because there is more than one unknown to be optimized in Eqs. (6) or (7), because the expressions of our problem in Eqs. (6) and (7) are nonlinear, and because it is possible to find some ranges for the lower and upper bounds of unknowns in Eqs. (6) and (7), in this paper, we will apply the "fmincon" function of MATLAB® [74], as one of the nonlinear minimization functions, for our multidimensional constrained nonlinear minimization problem. For the determination of the ranges of some unknowns, we could directly utilize the dependences of electromagnetic properties shown in Figs. 7 and 8 in addition to physical bounds of δ_e and δ_m. For example, for SB SRR and Composite MM slabs we can set

$$1 \le \varepsilon_\infty \le 5, \quad 0 \le \delta_e, \delta_m \le 5, \quad 1 \le \mu_s \le 2. \quad (8)$$

In addition, using the critical frequencies for homogenized SB&DB Composite MM slabs which yield $\varepsilon_r' = 0$ and $\mu_r' = 0$ from the dependences in Figs. 7 and 8 and from the dispersive model expressions in Eqs. (6) and (7), we determine the ranges of ω_{ep} and ω_{mp} as

$$\omega_{ep} \cong +\sqrt{\varepsilon_\infty\left(\omega_{er}^2 + \delta_e^2\right)}, \quad \omega_{mp} = \mp\sqrt{\frac{\omega_{mr}^2\left(\mu_s + \mu_\infty\right) \mp \sqrt{\omega_{mr}^4\left(\mu_s - \mu_\infty\right)^2 - 4\mu_\infty\mu_s\delta_m^2\omega_{mr}^2}}{2\mu_s}}, \quad (9)$$

where ω_{er} and ω_{mr} are the angular frequencies resulting in $\varepsilon_r' = 0$ and $\mu_r' = 0$ in Figs. 7 and 8, respectively. Due to finite accuracy of our simulation program (CST), we arranged the lower and upper bounds of ω_{ep} and ω_{mp} using a 5 percent offset criterion.

Following the procedure just discussed and applying the "fmincon" function of MATLAB, we extract the electromagnetic properties of the low-loss and lossy SB&DB

#174527 - $15.00 USD Received 17 Aug 2012; revised 15 Oct 2012; accepted 22 Oct 2012; published 13 Dec 2012

homogenized SRR and Composite MM cells whose details are presented in Section 3. In the analysis, after some optimization, we decided to use "Interior-point" algorithm and set the number of maximum iterations to 1,000 and maximum function evaluations to 10,000. Table 1 presents the optimized $\varepsilon_\infty, \omega_{ep}, \delta_e, \mu_\infty, \mu_s, \omega_{mp}$, and δ_m values for the analyzed lossy SB&DB SRR and Composite MM slabs, and Figs. 9, 10, 11, and 12 demonstrate the computed n, z, ε_r and μ_r over 6-14 GHz using the optimized values in Table 1.

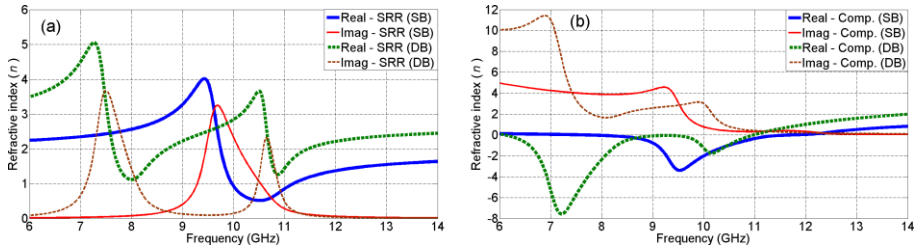

Fig. 9. Real and imaginary parts of retrieved refractive index of the lossy SB&DB (a) SRR MM slab and (b) Composite MM slab using the dispersion model approach.

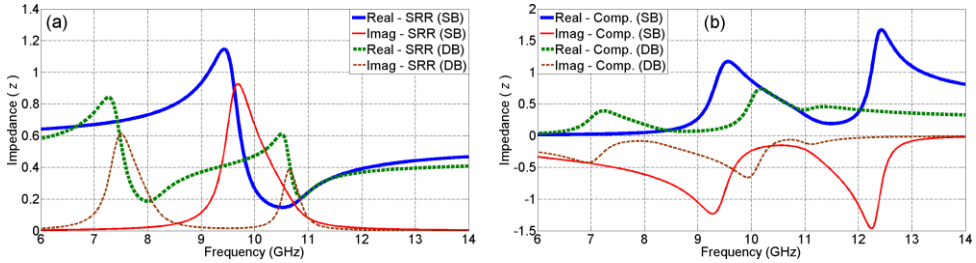

Fig. 10. Real and imaginary parts of retrieved wave impedance of the lossy SB&DB (a) SRR MM slab and (b) Composite MM slab using the dispersion model approach.

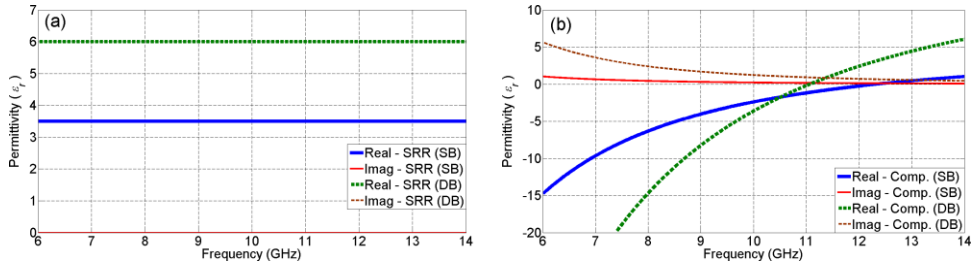

Fig. 11. Real and imaginary parts of retrieved permittivity of the lossy SB&DB (a) SRR MM slab and (b) Composite MM slab using the dispersion model approach.

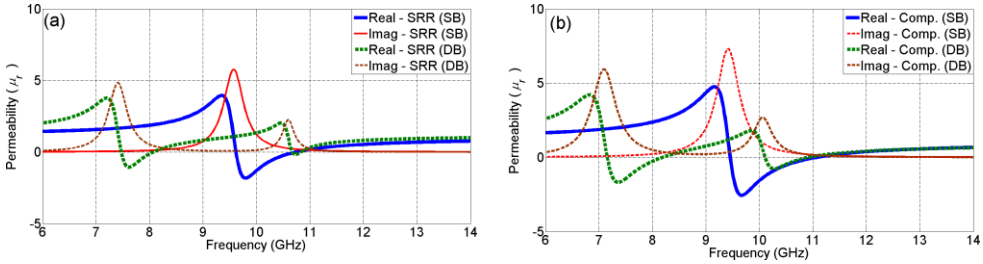

Fig. 12. Real and imaginary parts of retrieved permeability of the lossy SB&DB (a) SRR MM slab and (b) Composite MM slab using the dispersion model approach.

#174527 - $15.00 USD Received 17 Aug 2012; revised 15 Oct 2012; accepted 22 Oct 2012; published 13 Dec 2012

Table 1. Optimized Drude/Lorentz Dispersive Parameters for the Lossy SB&DB SRR and Compos. MM Slabs

Parameter	SB SRR	DB SRR	SB Composite	DB Composite
ε_∞	3.501	5.999	4.602	16.156
ω_{ep1} (GHz)	$2\pi \times 0$	$2\pi \times 0$	$2\pi \times 26.458$	$2\pi \times 32.364$
ω_{ep2} (GHz)	–	$2\pi \times 0$	–	$2\pi \times 30.637$
δ_{e1} (GHz)	–	–	2.017	3.944
δ_{e2} (GHz)	–	–	–	3.869
μ_{s1}	1.268	0.999	1.393	0.848
μ_{s2}	–	0.505	–	0.638
$\mu_{\infty 1}$	1.000	0.729	1.000	0.402
$\mu_{\infty 2}$	–	0.449	–	0.524
ω_{mp1} (GHz)	$2\pi \times 9.576$	$2\pi \times 7.412$	$2\pi \times 9.419$	$2\pi \times 7.100$
ω_{mp2} (GHz)	–	$2\pi \times 10.597$	–	$2\pi \times 10.064$
δ_{m1} (GHz)	2.788	2.595	3.177	3.358
δ_{m2} (GHz)	–	1.665	–	2.729

It is seen from Figs. 5–12 that the electromagnetic properties retrieved by the dispersion model approach are smoother than those by the analytical approach. This smoothing property resembles to that used for suppressing the Fabry-Perot artifacts arising from artificial Lorentzian poles [41]. Most importantly, we note from Figs. 7–12 that extracted $\varepsilon_r^{"}$ and $\mu_r^{"}$ of both lossy SB&DB SRR and Composite MM slabs by the dispersion model approach are in good agreement with the constraint on passive media ($\varepsilon_r^{"} > 0$ and $\mu_r^{"} > 0$), while those by the analytical model do not.

5. Uncertainty analysis

In the retrieval of electromagnetic properties in Figs. 5–12, we have assumed that there is not any inaccuracy in the measured S-parameters. However, in practical applications, the magnitude and phase of each S-parameter have some inaccuracies associated with them [75–79], and in turn these uncertainties may hinder accurate retrieval of electromagnetic properties of MM slabs. In addition, in most applications in the electromagnetic characterization of MM slabs, their thickness is arranged so that it is quite less than the operating wavelength in order to simplify the complexity of analysis (continuous medium approach). In this circumstance, the uncertainty in slab length measurements considerably increases even such measurements have been performed by a high precision micrometer. Finally, to fully characterize the properties of MM slabs (especially for multiband MM slabs [16,58,59]) near some specific frequency bands such as a band of negative refractive index, it is beneficial to take into consideration the uncertainty in the operating frequency. Since the electromagnetic properties of MM slabs are all linked to S-parameters, the slab length, and the operating frequency (see Eqs. (1)-(5)), any uncertainty in these quantities may seriously affect the retrieved electromagnetic properties. Accordingly, an appropriate metric tool considering the effects of any uncertainties in these parameters should be devised. The sensitivity analyses given in [37,57] do not attempt to analyze all these effects. Only a complete uncertainty analysis, which is overlooked in most MM retrieval methods based on S-parameters in the literature, can fill in this gap. Therefore, in this section, we apply a comprehensive uncertainty analysis for investigation the effects of uncertainties in S-parameters, the slab length, and the operating frequency on the retrieved electromagnetic properties of MM slabs in Figs. 1 and 2.

The differential uncertainty model, which examines the effect of minute changes in the independent variables on dependent ones, will be applied for our analysis [75–77,79–81]. In this model, a total differential is taken for each dependent variable (for our case, ε_r and μ_r) as functions of independent variables [for our case, the main factors contributing to the error budget are assumed to be $|S_{11}|$, $|S_{21}|$, θ_{11}, θ_{21}, d , and f]. Since the value of a term of the total differential of a dependent variable can be negative while others being positive or vice versa, each term of the total differential is first squared and then summed, and finally, the

#174527 - $15.00 USD Received 17 Aug 2012; revised 15 Oct 2012; accepted 22 Oct 2012; published 13 Dec 2012

summation is square-rooted. We also note that since our uncertainty analysis considers the total differential of a dependent variable, it is assumed that the dependent variables are analytic (or satisfy the Cauchy-Riemann equations [82,83]) over the region of interest with respect to the differentiation parameters. Following the procedure in [81], we find

$$\frac{\Delta\xi}{\xi}=\frac{1}{\xi}\sqrt{\sum_{u}\left[\left(\frac{\partial\xi}{\partial|S_u|}\Delta|S_u|\right)^2+\left(\frac{\partial\xi}{\partial\theta_u}\Delta\theta_u\right)^2\right]+\left(\frac{\partial\xi}{\partial d}\Delta d\right)^2+\left(\frac{\partial\xi}{\partial f}\Delta f\right)^2}, \quad (10)$$

where ξ stands for the real and imaginary parts of ε_r or μ_r and $u=11$ and 21. The partial derivatives in Eq. (10) are given as

$$\begin{aligned}\frac{\partial\varepsilon_r}{\partial|S_{11}|}&=\frac{De^{i\theta_{11}}}{AD-BC}, \quad \frac{\partial\varepsilon_r}{\partial|S_{21}|}=\frac{-Be^{i\theta_{21}}}{AD-BC},\\ \frac{\partial\varepsilon_r}{\partial d}&=\frac{DE-BF}{AD-BC}, \quad \frac{\partial\varepsilon_r}{\partial f}=\frac{DG-BH}{AD-BC},\end{aligned} \quad (11)$$

$$\begin{aligned}\frac{\partial\mu_r}{\partial|S_{11}|}&=-\frac{C}{D}\frac{\partial\varepsilon_r}{\partial|S_{11}|}, \quad \frac{\partial\mu_r}{\partial|S_{21}|}=-\frac{A}{B}\frac{\partial\varepsilon_r}{\partial|S_{21}|},\\ \frac{\partial\mu_r}{\partial d}&=\frac{E-A\partial\varepsilon_r/\partial d}{B}, \quad \frac{\partial\mu_r}{\partial f}=\frac{G-A\partial\varepsilon_r/\partial f}{B},\end{aligned} \quad (12)$$

$$\frac{\partial\varepsilon_r}{\partial\theta_u}=i\,|S_u|\frac{\partial\varepsilon_r}{\partial|S_u|}, \quad \frac{\partial\mu_r}{\partial\theta_u}=i\,|S_u|\frac{\partial\mu_r}{\partial|S_u|}, \quad A=\frac{\partial S_{11}}{\partial\Gamma}\frac{\partial\Gamma}{\partial\varepsilon_r}+\frac{\partial S_{11}}{\partial T}\frac{\partial T}{\partial\varepsilon_r}, \quad (13)$$

$$B=\frac{\partial S_{11}}{\partial\Gamma}\frac{\partial\Gamma}{\partial\mu_r}+\frac{\partial S_{11}}{\partial T}\frac{\partial T}{\partial\mu_r}, \quad C=\frac{\partial S_{21}}{\partial\Gamma}\frac{\partial\Gamma}{\partial\varepsilon_r}+\frac{\partial S_{21}}{\partial T}\frac{\partial T}{\partial\varepsilon_r}, \quad D=\frac{\partial S_{21}}{\partial\Gamma}\frac{\partial\Gamma}{\partial\mu_r}+\frac{\partial S_{21}}{\partial T}\frac{\partial T}{\partial\mu_r}, \quad (14)$$

$$E=-\frac{\partial S_{11}}{\partial T}\frac{\partial T}{\partial d}, \quad F=-\frac{\partial S_{21}}{\partial T}\frac{\partial T}{\partial d}, \quad G=-\frac{\partial S_{11}}{\partial T}\frac{\partial T}{\partial f}, \quad H=-\frac{\partial S_{21}}{\partial T}\frac{\partial T}{\partial f}. \quad (15)$$

Since the explicit expressions in Eqs. (10)-(15) require the values of ε_r and μ_r for their evaluation, we utilize the retrieved electromagnetic properties by the analytical and dispersive model approaches (some are given in Figs. 5–12 in Section IV). Then, we draw the dependence of $\Delta\xi/\xi$ over frequency using those retrieved values.

5.1. Uncertainties in S-parameters

Figures 13, 14, 15, 16, 17, and 18 demonstrate, respectively, the dependences $\Delta\varepsilon_r/\varepsilon_r$ and $\Delta\mu_r/\mu_r$ over $f=6-14$ GHz for the lossy SB&DB SRR and Composite MM slabs, and the same dependences for the low-lossq and lossy SB Composite MM slabs. It is noted from Fig. 15(a) that for SB&DB SRR slabs, only the dependence $\Delta\varepsilon_r$ is shown since $\varepsilon_r^{"}$ is set to zero by the dispersion model approach. To better interpret these dependences, we also illustrate important largest uncertainty levels and their reasons for both the lossy SB&DB SRR and Composite MM slabs in Tables 2 and 3. Here, the errors due to S-parameters are taken as $\Delta|S_{11}|=\Delta|S_{21}|=0.0025$ and $\Delta\theta_{11}=\Delta\theta_{21}=0.025^{o}$, $\Delta d=0$, and $\Delta f=0$.

#174527 - $15.00 USD Received 17 Aug 2012; revised 15 Oct 2012; accepted 22 Oct 2012; published 13 Dec 2012

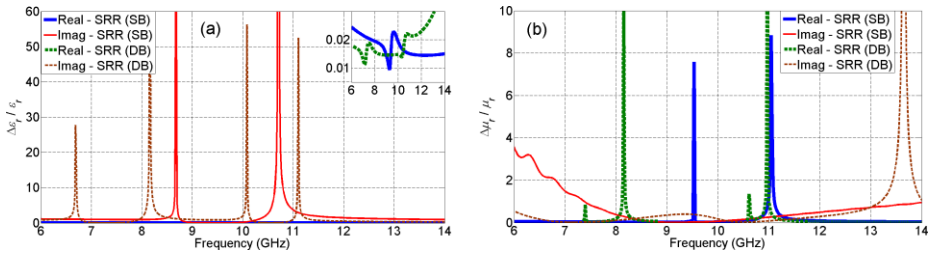

Fig. 13. Frequency dependence of real and imaginary parts of (a) $\Delta\varepsilon_r/\varepsilon_r$ and (b) $\Delta\mu_r/\mu_r$ for the lossy SB&DB SRR MM slabs using the analytical approach.

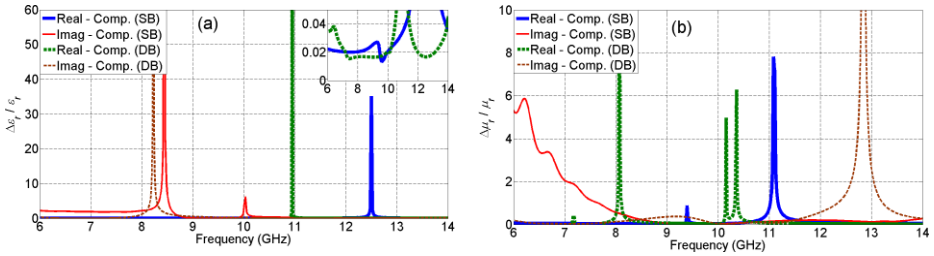

Fig. 14. Frequency dependence of real and imaginary parts of (a) $\Delta\varepsilon_r/\varepsilon_r$ and (b) $\Delta\mu_r/\mu_r$ for the lossy SB&DB Composite MM slabs using the analytical approach.

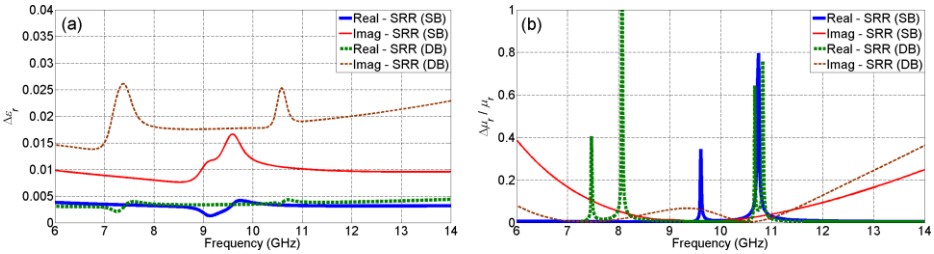

Fig. 15. Frequency dependence of real and imaginary parts of (a) $\Delta\varepsilon_r$ and (b) $\Delta\mu_r/\mu_r$ for the lossy SB&DB SRR MM slabs using the dispersive model approach.

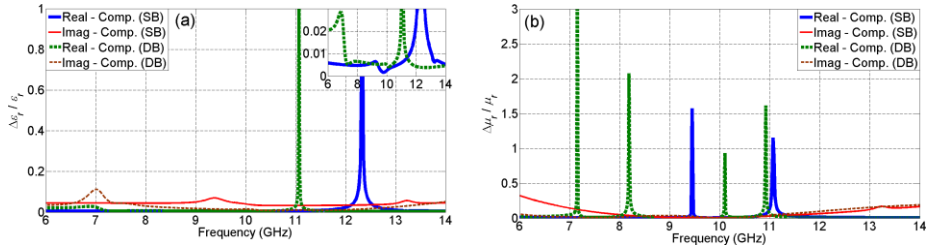

Fig. 16. Frequency dependence of real and imaginary parts of (a) $\Delta\varepsilon_r/\varepsilon_r$ and (b) $\Delta\mu_r/\mu_r$ for the lossy SB&DB Composite MM slabs using the dispersive model approach.

#174527 - $15.00 USD Received 17 Aug 2012; revised 15 Oct 2012; accepted 22 Oct 2012; published 13 Dec 2012

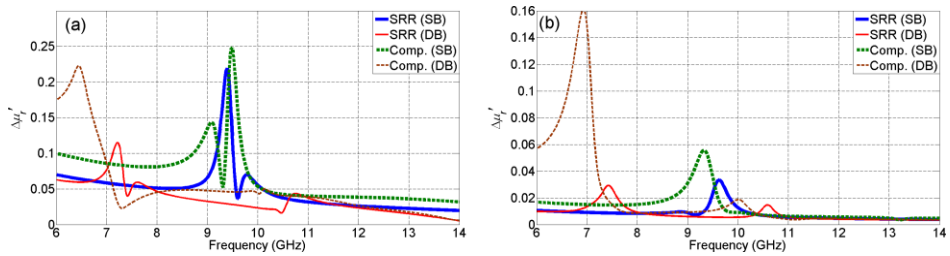

Fig. 17. Frequency dependence of $\Delta\mu_r^{'}$ for lossy SB&DB SRR and Composite MM slabs obtained from (a) the analytical approach and (b) the dispersive model approach.

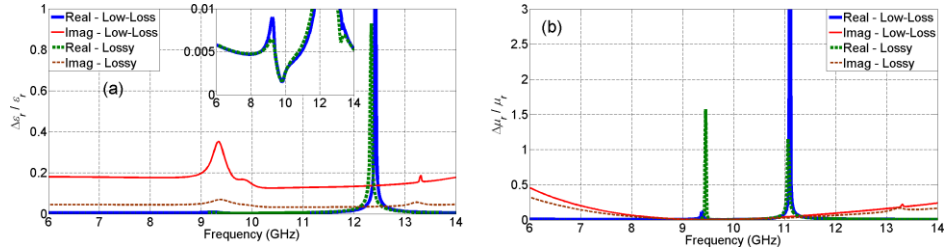

Fig. 18. Frequency dependence of real and imaginary parts of (a) $\Delta\varepsilon_r/\varepsilon_r$ and (b) $\Delta\mu_r/\mu_r$ for the low-loss and lossy SB Composite MM slabs using the dispersive model approach.

Table 2. Important Largest Uncertainty Levels and their Reasons for the Lossy SB&DB SRR MM Slabs (the Number in Parentheses in a Superscript Denotes the Reason of Uncertainty Level)

Slab prop.		Term	Analytical Approach	Dispersion Model Approach
SRR (Lossy)	Single-band [Figs. 13 and 15]	$\Delta\varepsilon_r^{'}/\varepsilon_r^{'}$	0.03 at ~9.58 GHz$^{(2)}$ [Fig. 13(a)]	0.005 at ~9.58 GHz$^{(2)}$ [Fig. 15(a)]
		$\Delta\varepsilon_r^{''}/\varepsilon_r^{''}$	>60 at ~8.7 GHz$^{(1)}$, >60 at ~10.7 GHz$^{(1)}$ [Fig. 13(a)]	0.017 at ~9.58 GHz$^{(2)}$ [Fig. 15(a)]
		$\Delta\mu_r^{'}/\mu_r^{'}$	8 at ~9.58 GHz$^{(1),(2)}$, 9 at ~11.1 GHz$^{(1)}$ [Fig. 13(b)]	0.35 at ~9.58 GHz$^{(1),(2)}$, 0.8 at ~10.9 GHz$^{(1)}$ [Fig. 15(b)]
		$\Delta\mu_r^{''}/\mu_r^{''}$	4 over 6-8 GHz$^{(1)}$ [Fig. 13(b)]	0.4 over 6-8 GHz$^{(1)}$, 0.3 over 12-14 GHz$^{(1)}$ [Fig. 15(b)]
	Dual-band [Figs. 13 and 15]	$\Delta\varepsilon_r^{'}/\varepsilon_r^{'}$	0.030 at ~7.41 GHz$^{(2)}$, 0.040 at ~10.6 GHz$^{(2)}$ [Fig. 13(a)]	0.004 at ~7.41 GHz$^{(2)}$, 0.004 at ~10.6 GHz$^{(2)}$ [Fig. 15(a)]
		$\Delta\varepsilon_r^{''}/\varepsilon_r^{''}$	27.7 at ~6.7 GHz$^{(1)}$, >60 at ~8.17 GHz$^{(1)}$ 57.1 at ~10.1 GHz$^{(1)}$, 52.5 at ~11.0 GHz$^{(1)}$ [Fig. 13(a)]	0.026 at ~7.41 GHz$^{(2)}$, 0.025 at ~10.6 GHz$^{(2)}$ [Fig. 15(a)]
		$\Delta\mu_r^{'}/\mu_r^{'}$	0.87 at ~7.41 GHz$^{(1),(2)}$, 10.5 at ~8.17 GHz$^{(1)}$ 1.35 at ~10.6 GHz$^{(1),(2)}$, 16.9 at ~11.0 GHz$^{(1)}$ [Fig. 13(b)]	0.41 at ~7.41 GHz$^{(1),(2)}$, 1.38 at ~8.17 GHz$^{(1)}$ 0.65 at ~10.6 GHz$^{(1),(2)}$, 0.76 at ~10.83 GHz$^{(1)}$ [Fig. 15(b)]
		$\Delta\mu_r^{''}/\mu_r^{''}$	>60 at ~13.65 GHz$^{(1)}$ [Fig. 13(b)]	0.08 over 6-8 GHz$^{(1)}$, 0.38 over 12-14 GHz$^{(1)}$ [Fig. 15(b)]

#174527 - $15.00 USD Received 17 Aug 2012; revised 15 Oct 2012; accepted 22 Oct 2012; published 13 Dec 2012

Table 3. Important Largest Uncertainty Levels and their Reasons for the Lossy SB&DB Composite MM Slabs (the Number in Parentheses in a Superscript Denotes the Reason of Uncertainty Level)

Slab prop.		Term	Analytical Approach	Dispersion Model Approach
Composite (Lossy)	Single-band [Figs. 14 and 16]	$\Delta\varepsilon_r'/\varepsilon_r'$	35.2 at ~12.5 GHz$^{(1)}$ [Fig. 14(a)]	0.93 at ~12.47 GHz$^{(1)}$ [Fig. 16(a)]
		$\Delta\varepsilon_r''/\varepsilon_r''$	>60 at ~8.41 GHz$^{(1)}$, 6.3 at ~10.0 GHz$^{(1)}$ [Fig. 14(a)]	0.07 at ~9.38 GHz$^{(2)}$ [Fig. 16(a)]
		$\Delta\mu_r'/\mu_r'$	0.88 at ~9.39 GHz$^{(1),(2)}$, 7.83 at ~11.1 GHz$^{(1)}$ [Fig. 14(b)]	1.57 at ~9.43 GHz$^{(1),(2)}$, 1.15 at ~11.1 GHz$^{(1)}$ [Fig. 16(b)]
		$\Delta\mu_r''/\mu_r''$	6 over 6-8 GHz$^{(1)}$ [Fig. 14(b)]	0.4 over 6-8 GHz$^{(1)}$, 0.3 over 12-14 GHz$^{(1)}$ [Fig. 16(b)]
	Dual-band [Figs. 14 and 16]	$\Delta\varepsilon_r'/\varepsilon_r'$	0.04 at ~7.25 GHz$^{(2)}$, >60 at ~11.0 GHz$^{(1)}$ [Fig. 14(a)]	0.004 at ~7.28 GHz$^{(2)}$, 0.004 at ~11.0 GHz$^{(1)}$ [Fig. 16(a)]
		$\Delta\varepsilon_r''/\varepsilon_r''$	>60 at ~8.2 GHz$^{(1)}$ [Fig. 14(a)]	0.027 at ~7.41 GHz$^{(2)}$, 1.039 at ~11.0 GHz$^{(2)}$ [Fig. 16(a)]
		$\Delta\mu_r'/\mu_r'$	0.43 at ~7.25 GHz$^{(1),(2)}$, 11.55 at ~8.1 GHz$^{(1)}$ 4.98 at ~10.16 GHz$^{(1),(2)}$, 6.29 at ~10.36 GHz$^{(1)}$ [Fig. 14(b)]	3.6 at ~7.24 GHz$^{(1),(2)}$, 2.1 at ~8.17 GHz$^{(1)}$ 0.93 at ~10.12 GHz$^{(1),(2)}$, 1.62 at ~10.92 GHz$^{(1)}$ [Fig. 16(b)]
		$\Delta\mu_r''/\mu_r''$	>60 at ~12.84 GHz$^{(1)}$ [Fig. 14(b)]	0.24 over 12-14 GHz$^{(1)}$ [Fig. 16(b)]

From the dependences $\Delta\varepsilon_r/\varepsilon_r$ and $\Delta\mu_r/\mu_r$ in Figs. 13–18 and from the data in Tables 2 and 3, we note the following important results.

1) The dependences of both real and imaginary parts of $\Delta\varepsilon_r/\varepsilon_r$ and $\Delta\mu_r/\mu_r$ drastically increase at some frequency ranges due to relatively small (approximately zero) values of ε_r and μ_r which directly enter into the expression of the denominator of Eq. (10). This increase completely depends on how small the values of ε_r and μ_r are and is denoted as the first reason of larger dependences in Tables 2 and 3. For instance, it is seen from Figs. 14(a) and 16(a) that the dependence $\Delta\varepsilon_r'/\varepsilon_r'$ of the lossy SB Composite MM slab determined from analytical and dispersive models is relatively lower over the whole frequency band except for $f\cong 12.5$ GHz which corresponds to a zero value of ε_r' for the Composite MM slab as seen from Figs. 7(b) and 11(b). On the other hand, for example, it is noticed from Figs. 13(b) and 15(b) and Table 2 that values of the dependence $\Delta\mu_r'/\mu_r'$ of the lossy DB SRR MM slab determined from analytical and dispersive models approximately at $f\cong 7.41$ GHz and $f\cong 10.6$ GHz are significantly lower than those nearly at $f\cong 8.17$ GHz and $f\cong 11.0$ GHz. This discrepancy comes from the fact that at some frequencies the values of ε_r and μ_r drastically decrease to zero, while at other frequencies their values are comparatively larger than, but still approximately zero. In general, we can state that the value of the analyzed dependence of a MM slab is relatively larger at frequencies where that dependence slowly varies with frequency (smaller frequency rate (derivative/slope) of that dependence).

2) The dependences $\Delta\varepsilon_r/\varepsilon_r$ and $\Delta\mu_r/\mu_r$ noticeably increase when there result large variations in the magnitudes and phases of reflection and transmission S-parameters as shown in Figs. 3 and 4. This result is denoted as the second reason for larger

#174527 - $15.00 USD Received 17 Aug 2012; revised 15 Oct 2012; accepted 22 Oct 2012; published 13 Dec 2012

dependences in Tables 2 and 3. In particular, the uncertainties $\Delta\varepsilon_r^{'}/\varepsilon_r^{'}$ and $\Delta\mu_r^{'}/\mu_r^{'}$ (and also their imaginary parts) are perceptible at approximately $f \cong 7.2$ GHz and $f \cong 10.1$ GHz for the lossy DB Composite MM slab, as can be seen from the insets in Figs. 14(a) and 16(a) and also from Table 1. These frequency regions correspond to the resonance regions of the lossy DB Composite MM slab, and fast changes within those regions are the main characteristics of MM slabs just like any other resonating structures [67] such as series or parallel RLC resonant (lump parameter) circuit [68], transmission-lines (distributed parameters) with lengths of $\lambda/2$ and $\lambda/4$ [60], Fabry-Perot resonators [69], and cavity resonators [60].

3) The increased value of the analyzed dependences $\Delta\varepsilon_r/\varepsilon_r$ and/or $\Delta\mu_r/\mu_r$ at some frequencies due to the second reason is remarkably lower than that due to the first reason. For example, Figs. 17(a) and 17(b) demonstrate the dependence $\Delta\mu_r^{'}$ of lossy SB&DB SRR and Composite MM slabs extracted from analytical and dispersive model approaches. Comparison the dependences in Fig. 17 with those in Figs. 13(b)-16(b) indicates that the effect of approximately zero value of μ_r significantly alters the uncertainty $\Delta\mu_r/\mu_r$. This circumstance is also valid for the uncertainty $\Delta\varepsilon_r/\varepsilon_r$ in which the dependence $\Delta\varepsilon_r^{'}$ for different MM slabs is not shown for brevity.

4) While the dependences $\Delta\varepsilon_r^{''}/\varepsilon_r^{''}$ and $\Delta\mu_r^{''}/\mu_r^{''}$ of the lossy SB&DB SRR and Composite MM slabs obtained from the analytical approach drastically increase at some frequency regions, the same dependences obtained from the dispersive model do not have any large value at all at those frequencies. As an example of this, from Figs. 14(a) and 16(a) we note that the dependence $\Delta\varepsilon_r^{''}/\varepsilon_r^{''}$ of lossy DB Composite MM slab determined from the analytical approach extremely increases approximately at 8.2 GHz corresponding with $\varepsilon_r^{''} \cong 0$ as seen from Fig. 7(b), whereas that from the dispersion model does not. This circumstance arises from the fact that the CST simulation program utilized in our analysis has finite accuracy in simulations (as other simulation programs) and that while analytical model does not consider the constraint $\varepsilon_r^{''} \geq 0$, the dispersive model does.

5) Results given between 1) and 4) for lossy MM slabs are also valid for low-loss MM slabs.

6) As seen from Figs. 18(a) and 18(b), an increase of loss factor, arising from an increase due to imperfect dielectric used as a substrate as well as finite conductivity of metals, of the SB&DB Composite MM slabs accompanies with a decrease of the overall uncertainty in the determination of ε_r and μ_r. This point is linked to the above second point since any loss present inside a resonating structure diminishes the number of radians through which the lossy structure oscillates as its energy decays to $1/e$ of its initial amplitude [84] and thus decreases the quality factor, limiting a rapid change in the measured S-parameters as well as ε_r and μ_r values.

5.2. Uncertainties in slab thickness and operating frequency

For the dependences in Figs. 13–18, we considered that $\Delta d = 0$ and $\Delta f = 0$. Now we focus on monitoring the dependences $\partial\xi/\partial d$ and $\partial\xi/\partial f$ over frequency. For example, Figs. 19, 20, 21, 22, 23, and 24 demonstrate, respectively, the dependences $\partial\varepsilon_r/\partial d$, $\partial\mu_r/\partial d$,

#174527 - $15.00 USD Received 17 Aug 2012; revised 15 Oct 2012; accepted 22 Oct 2012; published 13 Dec 2012

$\partial\varepsilon_r/\partial f$, and $\partial\mu_r/\partial f$ over $f = 6-14$ GHz for the lossy SB&DB Composite MM slabs, and the same dependences for the low-loss and lossy SB Composite MM slab, since these slabs demonstrate negative refractive indices over some certain frequency band(s).

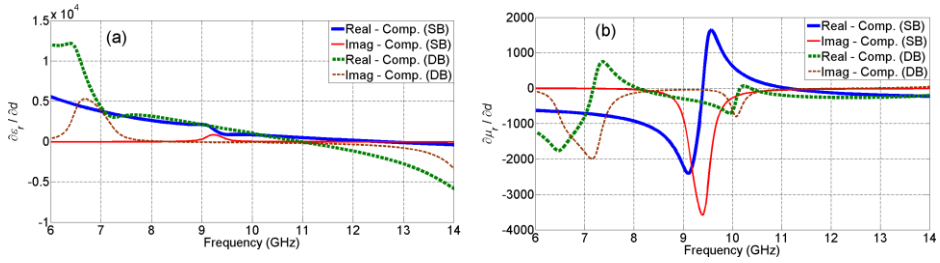

Fig. 19. Frequency dependence of real and imaginary parts of (a) $\partial\varepsilon_r/\partial d$ and (b) $\partial\mu_r/\partial d$ for the lossy SB&DB Composite MM slabs using the analytical approach.

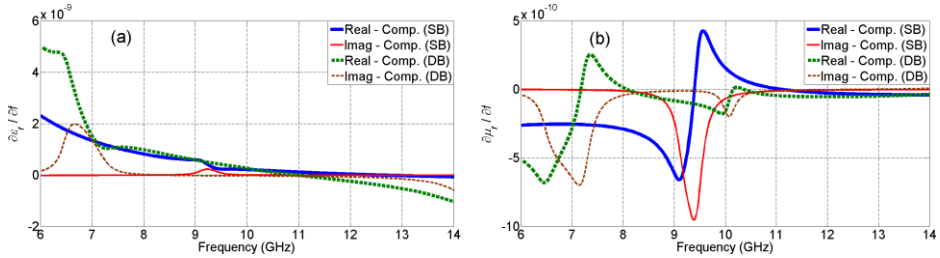

Fig. 20. Frequency dependence of real and imaginary parts of (a) $\partial\varepsilon_r/\partial f$ and (b) $\partial\mu_r/\partial f$ for the lossy SB&DB Composite MM slabs using the analytical approach.

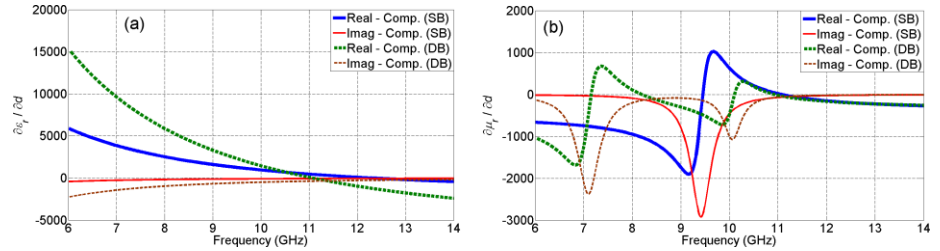

Fig. 21. Frequency dependence of real and imaginary parts of (a) $\partial\varepsilon_r/\partial d$ and (b) $\partial\mu_r/\partial d$ for the lossy SB&DB Composite MM slabs using the dispersive model approach.

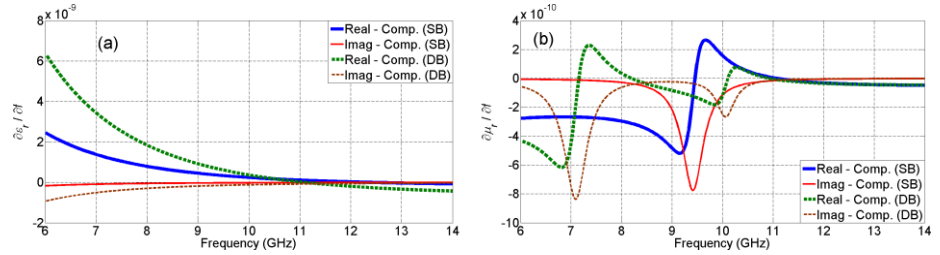

Fig. 22. Frequency dependence of real and imaginary parts of (a) $\partial\varepsilon_r/\partial f$ and (b) $\partial\mu_r/\partial f$ for the lossy SB&DB Composite MM slabs using the dispersive model approach.

#174527 - $15.00 USD Received 17 Aug 2012; revised 15 Oct 2012; accepted 22 Oct 2012; published 13 Dec 2012

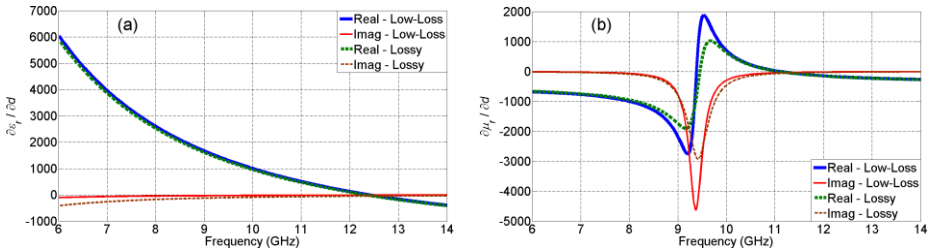

Fig. 23. Frequency dependence of real and imaginary parts of (a) $\partial\varepsilon_r/\partial d$ and (b) $\partial\mu_r/\partial d$ for the low-loss and lossy SB Composite MM slabs using the dispersive model approach.

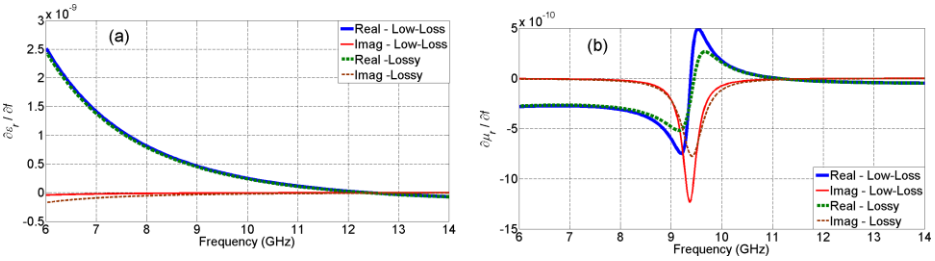

Fig. 24. Frequency dependence of real and imaginary parts of (a) $\partial\varepsilon_r/\partial f$ and (b) $\partial\mu_r/\partial f$ for the low-loss and lossy SB Composite MM slabs using the dispersive model approach.

From the dependences in Figs. 18–24, we note the following key results.

1) The Fabry-Perot artifacts, arising from artificial Lorentzian poles [41], of $\partial\varepsilon_r/\partial d$ and $\partial\varepsilon_r/\partial f$ by the analytical approach are removed by the dispersive model approach. For example, the artifacts of $\partial\varepsilon_r/\partial d$ and $\partial\varepsilon_r/\partial f$ for the lossy SB Composite MM slab near 9.5 GHz in Figs. 19(a) and 20(a) are removed in Figs. 21(a) and 22(a).

2) Superfluous resonating behaviors of $\partial\mu_r/\partial d$ and $\partial\mu_r/\partial f$ obtained from the analytical approach are eliminated (smoothed) by the dispersion model approach. In particular, it is seen from Figs. 21(b) and 22(b) that values of the dependences $\partial\mu_r/\partial d$ and $\partial\mu_r/\partial f$ are lower than those in Figs. 19(b) and 20(b).

3) The dependences $\partial\varepsilon_r/\partial d$, $\partial\varepsilon_r/\partial f$, $\partial\mu_r/\partial d$, and $\partial\mu_r/\partial f$ in Figs. 19–22 extracted from analytical and dispersive model approaches for the lossy SRR and Composite MM slabs exhibit similar behaviors and patterns contrary to the dependences $\Delta\varepsilon_r/\varepsilon_r$ and/or $\Delta\mu_r/\mu_r$ in Figs. 13–16. This difference mainly comes from the effect of inclusion of four uncertainty parameters $\partial\xi/\partial|S_{11}|$, $\partial\xi/\partial|S_{21}|$, $\partial\xi/\partial|\theta_{11}|$, and $\partial\xi/\partial|\theta_{21}|$ into the uncertainty analysis of each $\Delta\varepsilon_r/\varepsilon_r$ and/or $\Delta\mu_r/\mu_r$ dependence while $\partial\varepsilon_r/\partial d$, $\partial\varepsilon_r/\partial f$, $\partial\mu_r/\partial d$, and $\partial\mu_r/\partial f$ are only considered as themselves and individual in the uncertainty analysis.

4) Values of the dependences $\partial\varepsilon_r/\partial f$ and $\partial\mu_r/\partial f$ in Figs. 20 and 22 are significantly lower (or negligible on practical grounds) than those $\partial\varepsilon_r/\partial d$ and $\partial\mu_r/\partial d$ in Figs. 19 and 21. This effect is a result of dominant or insignificant relative changes in operating frequency and slab length over their nominal values in the expression of

#174527 - $15.00 USD Received 17 Aug 2012; revised 15 Oct 2012; accepted 22 Oct 2012; published 13 Dec 2012

T in Eq. (2). For example, while a 5 percent change in a slab length of $d = 2.5$ mm is perceivable and effective in the dependences $\partial\varepsilon_r/\partial d$ and $\partial\mu_r/\partial d$, the same change in operating frequency of $f = 10$ GHz is not much sensible. Nonetheless, for MM slabs resonating at lower frequencies and having larger MM slab lengths, dependences $\partial\varepsilon_r/\partial f$ and $\partial\mu_r/\partial f$ become significant and should be taken into account in the error budget.

5) The results given between 1) and 4) for lossy Composite MM slabs are also valid for low-loss SRR and Composite MM slabs as well as lossy SRR MM slabs.

6) The impact of slab losses alters the dependences $\partial\varepsilon_r/\partial d$, $\partial\varepsilon_r/\partial f$ and especially for $\partial\mu_r/\partial d$ and $\partial\mu_r/\partial f$ near resonance frequencies (Figs. 23 and 24). This means that accurate knowledge of MM slab length as well as the operating frequency is a prerequisite for accurate retrieval of exotic electromagnetic properties (such as negative n) of MM slabs, especially for multiband MM slabs [16,58,59].

6. Conclusion

A complete uncertainty analysis has been performed to monitor the dependences on retrieved electromagnetic properties of MM slabs. Two different slabs composed of only SRR (SRR MM slab) and of SRR with a continuous wire (Composite MM slab) with SB&DB properties are utilized for this purpose. We applied two different techniques to extract the electromagnetic properties of these slabs with different loss factors. While the first technique (analytical approach) retrieves the electromagnetic properties quicker, sometimes retrieved complex permittivity by this technique in resonance regions does not comply with passivity requirement for passive materials when the accuracy of employed simulation program is not so high. In fact, the number of lines per wavelength in the spatial discretization of the cubic SRR should be high enough to ensure that the transit time of the signal over the computation cell is much shorter than the characteristic times of the physical processes which occur inside the SRR to avoid numerical artifacts and non-causal effects. Analogously, in the time discretization the time step should be much smaller than the transit time along the cells to guarantee numerical stability and control parasitic oscillations. Then to provide accurate responses the computer running time becomes prohibitively large. Besides, the second technique (dispersion model approach) does remove these accuracies for the sake of increased time and of complexity in using an optimization algorithm. In our uncertainty analysis, after extracting the electromagnetic properties of the low-loss and lossy SB&DB SRR and Composite MM slabs using two approaches, we applied a differential uncertainty model, as a versatile uncertainty analysis method used for the analysis of conventional materials, to examine the dependences of retrieved electromagnetic properties of MM slabs on the uncertainties in S-parameters, the slab length as well as the operating frequency. Our uncertainty analysis shows that when either the values of retrieved electromagnetic properties approach to zero or measured/simulated S-parameters have a sharp change over frequency such as negative refractive index region, the uncertainty in extracted electromagnetic properties of MM slabs significantly increases. Any low-loss or medium-low present in the MM slabs decreases the uncertainties in electromagnetic properties arising from abrupt changes in measured/simulated S-parameters. Finally, we note that exact information about especially the slab length together with the operating frequency is an essential parameter to investigate the correct and exotic electromagnetic features of SRR and Composite MM slabs.

#174527 - $15.00 USD Received 17 Aug 2012; revised 15 Oct 2012; accepted 22 Oct 2012; published 13 Dec 2012